

Superfluidity and pairing phenomena in ultracold atomic Fermi gases in one-dimensional optical lattices. II. Effects of population imbalance

Jibiao Wang,^{1,2} Lin Sun,² Qiang Zhang,² Leifeng Zhang,² Yi Yu,³ Chaohong Lee ^{1,4} and Qijin Chen ^{5,2,6,*}

¹Guangdong Provincial Key Laboratory of Quantum Metrology and Sensing & School of Physics and Astronomy, Sun Yat-Sen University (Zhuhai Campus), Zhuhai, Guangdong 519082, China

²Department of Physics and Zhejiang Institute of Modern Physics, Zhejiang University, Hangzhou, Zhejiang 310027, China

³College of Chemical Engineering, Zhejiang University of Technology, Hangzhou, Zhejiang 310014, China

⁴State Key Laboratory of Optoelectronic Materials and Technologies, Sun Yat-Sen University (Guangzhou Campus), Guangzhou, Guangdong 510275, China

⁵Shanghai Branch, National Laboratory for Physical Sciences at Microscale and Department of Modern Physics, University of Science and Technology of China, Shanghai 201315, China

⁶Synergetic Innovation Center of Quantum Information and Quantum Physics, Hefei, Anhui 230026, China



(Received 15 January 2020; accepted 7 April 2020; published 11 May 2020)

In this paper, we study the effect of population imbalance and its interplay with pairing strength and lattice effect in atomic Fermi gases in a one-dimensional optical lattice. We compute various phase diagrams as the system undergoes BCS-BEC crossover, using the same pairing fluctuation theory as in Part I of this work [Phys. Rev. A **101**, 053617 (2020)]. We find widespread pseudogap phenomena beyond the BCS regime and intermediate temperature superfluid states for relatively low population imbalances. The Fermi surface topology plays an important role in the behavior of T_c . For large d and/or small t , which yield an open Fermi surface, superfluidity can be readily destroyed by a small amount of population imbalance p . The superfluid phase, especially in the BEC regime, can exist only for a highly restricted volume of the parameter space. An open Fermi surface often leads to destruction of the superfluid ground state in the BEC regime. Due to the continuum-lattice mixing, population imbalance gives rise to a new mechanism for pair hopping, as assisted by excessive majority fermions, which may lead to significant enhancement of T_c on the BEC side of the Feshbach resonance, and also render T_c approaching a constant asymptote in the BEC limit, when it exists. Furthermore, we find that not all minority fermions will be paired up in BEC limit, unlike the 3D continuum case. These predictions can be tested in future experiments.

DOI: [10.1103/PhysRevA.101.053618](https://doi.org/10.1103/PhysRevA.101.053618)

I. INTRODUCTION

With multiple experimentally tunable parameters, ultracold atomic Fermi gases and optical lattices have attracted enormous attention [1–3]. Fermions in optical lattices are often described by a Hubbard model [2–4]. Among them, the one-dimensional (1D) optical lattices have been realized experimentally for a long time [5–7]. However, a proper treatment of fermions in 1D optical lattices is not yet available, since most theoretical in this regard addresses pure lattice cases [8–13]. Theoretical studies on such a true 1D optical lattice in the experimental sense have been scarce. Devreese *et al.* studied possible Fulde-Ferrell-Larkin-Ovchinnikov (FFLO) states [14,15] in such a 1D optical lattice [16–18], but mostly restricted to the BCS and crossover regimes. Indeed, the superfluid and pairing physics in a 1D optical lattice has not been adequately studied thus far. In Part I of the present work [19], we have systematically studied the behavior of BCS-BEC crossover of atomic Fermi gases in a 1D optical lattice in the absence of a population (and mass) imbalance. In particular,

we have found widespread pseudogap phenomena, which bear strong signatures in single particle excitation spectrum and the superfluid density.

In this paper, we continue from Part I of this work [19] and study the effects of population imbalance and its interplay with lattice constant d and lattice hopping parameter t , besides the interaction strength and temperature, within the framework of the same pairing fluctuation theory. We find that the exponential behaviors of the fermionic chemical potential μ and the pairing gap Δ as a function of pairing strength in the BEC regime remain the same as in the balanced case. The behavior of the superfluid transition temperature T_c is largely governed by the Fermi surface topology. For large d and/or small t , which lead to an open Fermi surface, a small amount of population imbalance p may readily destroy superfluidity. Furthermore, the mixing between continuum and discrete lattice dimensions has more profound consequences than in the balanced case; the excessive majority fermions can assist pair hopping, providing a new pair hopping mechanism, which dominates the hopping via virtual pair unbinding [20] in the BEC regime. Together with the quasi-two dimensionality, which yields a constant ratio Δ^2/μ in the BEC limit, this new mechanism leads to a constant asymptote for T_c

*qchen@zju.edu.cn

for a BEC superfluid (when a BEC solution exists) in the presence of population imbalance. We shall present detailed T - p (temperature versus polarization) phase diagrams as the system undergoes the BCS-BEC crossover with different lattice constants and hopping integrals, and focus on the finite temperature and population imbalance effects, especially the pseudogap phenomena [21,22]. We shall also present T_c versus interaction strength $1/k_F a$ with varying lattice constants d , population imbalances p and hopping integrals t . As these phase diagrams reveal the following: (i) The superfluid phase exists only in a very restricted volume of the multidimensional parameter space; (ii) the pseudogap phenomena widely exist; (iii) intermediate temperature superfluidity is also a widespread phenomenon in the presence of population imbalance, similar to the homogeneous case [23–25], irrespective of the lattice constraint; (iv) a small population imbalance may greatly enhance the superfluidity by raising T_c on the BEC side of the Feshbach resonance; (v) a BEC superfluid exists only for a limited small volume in the parameter space of (t, d, p) ; (vi) while there is no superfluid ground state in the BCS and unitary regime, where it exists in the BEC regime is largely controlled by the Fermi surface topology (an open Fermi surface only leads to destruction of the zero T superfluid); and (vii) not all minority fermions will be paired when a BEC superfluid does exist.

II. THEORETICAL FORMALISM

In this section, we present briefly the theory, adapted for the population imbalanced case, with spin dependent chemical potential μ_σ and Green's functions $G_{0\sigma}(K)$ and $G_\sigma(K)$, with the (pseudo)spins $\sigma = \uparrow, \downarrow$. We keep the same notations as in Part I of this work [19].

We will present a set of equations which can be self-consistently solved for various quantities in different situations. In particular, we will show the relationship between the pseudogap and pairing fluctuations. In this process, we will show how the important pair dispersion is extracted in a self-consistent manner. In addition, we will discuss the stability of the solutions, which is always stable for the balanced case, and present the formula for the superfluid density. As in Part I of this work [19], we will also present our analytical result of the behavior of the system in the BEC regime.

A. Pairing fluctuation theory with a population imbalance

In this subsection, we shall recapitulate the pairing fluctuation theory and focus on the difference from Part I of this work [19], caused by the population imbalance. In particular, we shall present the set of self-consistent equations and how the pair dispersion is extracted.

The single particle dispersion is given by $\xi_{\mathbf{k}\sigma} = \mathbf{k}_\parallel^2/2m + 2t[1 - \cos(k_z d)] - \mu_\sigma \equiv \epsilon_{\mathbf{k}} - \mu_\sigma$. The bare Green's function is given by $G_{0\sigma}^{-1}(K) = i\omega_n - \xi_{\mathbf{k},\sigma}$, with the self-energy $\Sigma_\sigma(K) = \sum_Q t(Q)G_{0\bar{\sigma}}(Q-K)$, where $\bar{\sigma} = -\sigma$. The T -matrix $t(Q) = t_{sc}(Q) + t_{pg}(Q)$, where $t_{sc}(Q) = -(\Delta_{sc}^2/T)\delta(Q)$ vanishes for $T > T_c$, and $t_{pg}(Q) = U/[1 + U\chi(Q)]$, with the pair susceptibility $\chi(Q) = \sum_{K,\sigma} G_{0\sigma}(Q-K)G_{\bar{\sigma}}(K)/2$. The self-energy is given by $\Sigma_\sigma(K) = \Sigma_{sc,\sigma}(K) + \Sigma_{pg,\sigma}(K)$, where $\Sigma_{sc,\sigma}(K) =$

$-\Delta_{sc}^2 G_{0\bar{\sigma}}(-K)$, and $\Sigma_{pg,\sigma}(K) = \sum_Q t_{pg}(Q)G_{0\bar{\sigma}}(Q-K)$. At $T \leq T_c$, the BEC condition remains $t_{pg}^{-1}(Q=0) = U^{-1} + \chi(0) = 0$, and $\Sigma_{pg,\sigma}(K) \approx -\Delta_{pg}^2 G_{0\bar{\sigma}}(-K)$, with $\Delta_{pg}^2 \equiv -\sum_Q t_{pg}(Q)$. Then the total self-energy $\Sigma_\sigma(K) \approx -\Delta^2 G_{0\bar{\sigma}}(-K)$, where $\Delta^2 = \Delta_{sc}^2 + \Delta_{pg}^2$. Finally, the full Green's function becomes more complex due to population imbalance,

$$G_\sigma(K) = \frac{u_{\mathbf{k}}^2}{i\omega_n - E_{\mathbf{k}\sigma}} + \frac{v_{\mathbf{k}}^2}{i\omega_n + E_{\mathbf{k}\bar{\sigma}}}, \quad (1)$$

where $u_{\mathbf{k}}^2 = (1 + \xi_{\mathbf{k}}/E_{\mathbf{k}})/2$, $v_{\mathbf{k}}^2 = (1 - \xi_{\mathbf{k}}/E_{\mathbf{k}})/2$, $E_{\mathbf{k}\uparrow} = E_{\mathbf{k}} - h$, $E_{\mathbf{k}\downarrow} = E_{\mathbf{k}} + h$, and $E_{\mathbf{k}} = \sqrt{\xi_{\mathbf{k}}^2 + \Delta^2}$, $\xi_{\mathbf{k}} = \epsilon_{\mathbf{k}} - \mu$, $\mu = (\mu_\uparrow + \mu_\downarrow)/2$, $h = (\mu_\uparrow - \mu_\downarrow)/2$. From the number constraint $n_\sigma = \sum_{\mathbf{k}} G_\sigma(K)$, we can get the total fermion number density $n = n_\uparrow + n_\downarrow$ and the density difference $\delta n = n_\uparrow - n_\downarrow \equiv pn$,

$$n = \sum_{\mathbf{k}} \left[\left(1 - \frac{\xi_{\mathbf{k}}}{E_{\mathbf{k}}}\right) + 2\bar{f}(E_{\mathbf{k}}) \frac{\xi_{\mathbf{k}}}{E_{\mathbf{k}}} \right], \quad (2)$$

$$pn = \sum_{\mathbf{k}} [f(E_{\mathbf{k}\uparrow}) - f(E_{\mathbf{k}\downarrow})], \quad (3)$$

where $\bar{f}(x) = [f(x+h) + f(x-h)]/2$. Similar to the $p=0$ case, the extended gap equation is given by

$$\frac{m}{4\pi a} = \sum_{\mathbf{k}} \left[\frac{1}{2\epsilon_{\mathbf{k}}} - \frac{1 - 2\bar{f}(E_{\mathbf{k}})}{2E_{\mathbf{k}}} \right] + a_0\mu_p, \quad (4)$$

with $\mu_p = 0$ at $T \leq T_c$.

The inverse T -matrix expansion [1] remains formally the same as in the $p=0$ case, i.e., $t_{pg}^{-1}(\Omega, \mathbf{q}) \approx a_1\Omega^2 + a_0(\Omega - \Omega_{\mathbf{q}} + \mu_p)$, where $\Omega_{\mathbf{q}} = B_\parallel q_\parallel^2 + 2t_B[1 - \cos(q_z d)]$ with $B_\parallel = 1/2M_\parallel$, and all the coefficients a_1 , a_0 , B_\parallel , and t_B are determined automatically in the expansion process. Their concrete expressions are given by Eqs. (A4), (A5), and (A7) in the Appendix of Part I of this work [19] with the Fermi distribution functions $f(x)$ and $f'(x)$ replaced by $\bar{f}(x)$ and $\bar{f}'(x)$, respectively. The pseudogap equation is the same,

$$a_0\Delta_{pg}^2 = \sum_{\mathbf{q}} \frac{b(\tilde{\Omega}_{\mathbf{q}})}{\sqrt{1 + 4\frac{a_1}{a_0}(\Omega_{\mathbf{q}} - \mu_p)}}, \quad (5)$$

with the pair dispersion

$$\tilde{\Omega}_{\mathbf{q}} = \frac{\sqrt{a_0^2 + 4a_1 a_0(\Omega_{\mathbf{q}} - \mu_p)} - a_0}{2a_1}.$$

The pair density is given by $n_p = a_0\Delta^2$.

Equations (2)–(5) form a closed set of self-consistent equations, which can be used to solve for $(\mu_\uparrow, \mu_\downarrow, T^*)$ with $\Delta = 0$, for $(\mu_\uparrow, \mu_\downarrow, \Delta_{pg}, T_c)$ with $\Delta_{sc} = 0$, and for $(\mu_\uparrow, \mu_\downarrow, \Delta, \Delta_{pg})$ at $T < T_c$. Here the pair formation temperature T^* is approximated by the mean-field T_c , and the order parameter Δ_{sc} is derived from $\Delta_{sc}^2 = \Delta^2 - \Delta_{pg}^2$.

B. Stability analysis

From our previous work, it is known that, in the presence of population imbalance, not all solutions of Eqs. (2)–(5)

are stable. Therefore, in this subsection, we shall present a stability analysis of our solutions.

The stability analysis can be done following Ref. [26], as we summarize here. Consider the thermodynamic potential Ω_S , which consists of the fermionic (Ω_F) and bosonic (Ω_B) contributions,

$$\begin{aligned}\Omega_S &= \Omega_F + \Omega_B, \\ \Omega_F &= -\frac{\Delta^2}{U} + \sum_{\mathbf{k}} (\xi_{\mathbf{k}} - E_{\mathbf{k}}) - T \sum_{\mathbf{k}, \sigma} \ln(1 + e^{-E_{\mathbf{k}\sigma}/T}), \quad (6) \\ \Omega_B &= a_0 \mu_p \Delta_{pg}^2 + T \sum_{\mathbf{q}} \ln(1 - e^{-\tilde{\Omega}_{\mathbf{q}}/T}).\end{aligned}$$

The stability condition of population imbalanced Sarma phase [27] against phase separation (PS) can be simply expressed as

$$\frac{\partial^2 \Omega_S}{\partial \Delta^2} = 2 \sum_{\mathbf{k}} \frac{\Delta^2}{E_{\mathbf{k}}^2} \left[\frac{1 - 2\bar{f}(E_{\mathbf{k}})}{2E_{\mathbf{k}}} + \bar{f}'(E_{\mathbf{k}}) \right] > 0, \quad (7)$$

where $\bar{f}'(x) = d\bar{f}(x)/dx$. This condition is equivalent to the positive definiteness of the particle number susceptibility matrix $\{\partial n_{\sigma}/\partial \mu_{\sigma'}\}$ [26,28], which represents a form of generalized compressibility.

C. Superfluid density

Superfluid density, as a representative transport property, is an important quantity for the superfluid Fermi gas. The temperature dependence of the superfluid density depends crucially on the pairing symmetry and thus has been used to pinpoint the symmetry of the order parameter in the community of superconductivity. In the presence of population imbalanced, the superfluid density may become negative, signaling an instability of the superfluid solution [23,25,26]. Hence, the positive definiteness of the superfluid density is another, albeit weaker, stability condition [26].

Similar to the $p = 0$ case, the superfluid ‘‘density’’ (n_s/m), can also be derived using the linear response theory, following earlier works [23,26,29,30]. For the present contact potential, the superfluid density is given by

$$\left(\frac{n_s}{m}\right)_i = 2 \sum_{\mathbf{k}} \frac{\Delta_{sc}^2}{E_{\mathbf{k}}^2} \left[\frac{1 - \bar{f}(E_{\mathbf{k}})}{2E_{\mathbf{k}}} + \bar{f}'(E_{\mathbf{k}}) \right] \left(\frac{\partial \xi_{\mathbf{k}}}{\partial k_i} \right)^2, \quad (8)$$

where $i = x, y, z$ and $\bar{f}'(x) = d\bar{f}(x)/dx$.

As we will see below, the behavior of the superfluid density can become very usual for $p \neq 0$. Nevertheless, we expect the T dependence of both $(n_s/m)_{\parallel}$ and $(n_s/m)_{\perp}$ are close to each other.

D. Asymptotic behavior in the deep BEC regime

Analytical solutions can often be obtained in the weak and strong pairing limits, so that the physics can be made more transparent without resorting to complicated numerics. Following our practice in Part I of this work [19], in this subsection, we shall present the asymptotic behavior of population imbalanced atomic Fermi gases in 1DOL in the BEC regime. We find, both μ and Δ can be obtained analytically, while μ_{\uparrow} and T_c can be solved numerically using much simplified equations. Most importantly, we find that

population imbalance leads to extra terms in the coefficients of the expansion of the inverse T matrix, which become independent of the interaction strength and thus lead to a constant BEC asymptote for T_c .

Unlike the $p = 0$ case [19], in the presence of a population imbalance $p \neq 0$, the BEC limit is more complicated, as one can no longer obtain a complete analytical solution without resorting to numerics. However, one can still greatly reduce the complexity of the equations, as follows.

For $p = (n_{\uparrow} - n_{\downarrow})/n$, we consider $p > 0$, without loss of generality. The excessive majority fermions require $\mu_{\uparrow} > 0$ throughout the BCS-BEC crossover, whereas μ to leading order is roughly given by its balanced counterpart in the BEC limit, where the two-body physics dominates. Then μ_{\downarrow} is given by $\mu_{\downarrow} = 2\mu - \mu_{\uparrow}$. The size of $\mu_{\uparrow} > 0$ is determined by p , and $\mu_{\downarrow} \approx 2\mu \rightarrow -\infty$, so that $f(E_{\mathbf{k}}^{\downarrow}) = f(\xi_{\mathbf{k}}^{\downarrow}) = 0$. The Fermi function $f(E_{\mathbf{k}}^{\uparrow})$ no longer vanishes exponentially, and will lead to corrections to the equations above. Nevertheless, this Fermi function places a small finite energy and momentum cutoff, so that we have $E_{\mathbf{k}} \approx |\mu|$ to the leading order in many occasions. Thus, to leading-order corrections, the equation for total number density now becomes

$$(1 - p)n = -\frac{m\Delta^2}{4\pi\mu d} - \frac{np\Delta^2}{2\mu^2}, \quad (9)$$

$$\Delta = \sqrt{\frac{4\pi|\mu|d(1-p)n}{m} \left(1 - \frac{\pi dnp}{\mu m} \right)}. \quad (10)$$

Interestingly, the leading correction to Δ^2 is independent of $1/k_F a$, given by $8(\pi dn/m)^2(1-p)p$, which vanishes when $p = 0$. So is the correction term in Eq. (9).

Expanding $E_{\mathbf{k}}^{\uparrow}$, we have

$$E_{\mathbf{k}}^{\uparrow} = E_{\mathbf{k}} - h \approx \xi_{\mathbf{k}}^{\uparrow} - \frac{\Delta_{\mathbf{k}}^2}{2\mu} \approx \xi_{\mathbf{k}}^{\uparrow} + \frac{4\pi dn_{\downarrow}}{m}. \quad (11)$$

Note that the second term is again a constant for given p , independent of $1/k_F a$, precisely because $\Delta^2/\mu \rightarrow \text{const}$. For this reason, the difference $E_{\mathbf{k}}^{\uparrow} - \xi_{\mathbf{k}}^{\uparrow} = 4\pi dn_{\downarrow}/m$ will not approach 0 in the BEC limit, unlike the case in 3D continuum.

The equation of number difference is given by

$$pn = \sum_{\mathbf{k}} f(E_{\mathbf{k}}^{\uparrow}) = \sum_{\mathbf{k}} f\left(\xi_{\mathbf{k}}^{\uparrow} + \frac{4\pi dn_{\downarrow}}{m}\right) \equiv \frac{mt}{\pi^2 d} I_1. \quad (12)$$

Here the dimensionless integral I_1 depends on μ_{\uparrow} and T .

In comparison with the $p = 0$ case, the gap equation now also contains an extra term which is of the same order as the leading term in the BEC limit, namely,

$$\sum_{\mathbf{k}} \frac{f(E_{\mathbf{k}}^{\uparrow})}{2E_{\mathbf{k}}} \approx \frac{1}{2|\mu|} \sum_{\mathbf{k}} f(E_{\mathbf{k}}^{\uparrow}) = \frac{pn}{2|\mu|}, \quad (13)$$

Thus, without this term, the leading-order chemical potential is given by $\mu_0 = -te^{d/a}$, the same as in the $p = 0$ case, since the two-body physics dominates the deep BEC regime. The gap equation can now be simplified in a fashion similar to the $p = 0$ case, and we obtain

$$\mu = \mu_0 + 2t + \frac{2\pi dn_{\uparrow}}{m}, \quad (14)$$

formally identical to the expression for $p = 0$. Plugging Eq. (14) into Eq. (10), we can obtain the gap Δ . Note that for given (t, d, p) in the deep BEC regime, Eqs. (14) and (10) completely determines μ and Δ as a function of $1/k_F a$.

The relation between μ and d/a suggests that one can use μ as a tuning variable in experiment, while a simple general formula relating a and its 3D counterpart a_{3D} is not yet available. This is similar to the use of the binding energy ϵ_B as a tuning parameter for a 2D Fermi gas [31]. For detailed analysis, see Appendices A and B in Part I of this work [19].

As discussed in Part I of this work [19], the exponential behavior of μ and Δ as a function of $1/k_F a$ is an important feature of the quasi-two dimensionality of the present system; the ratio Δ^2/μ approaches a constant, independent of pairing strength. As we shall see below, this has important consequences. The (second and third) correction terms in Eq. (14) are also constants.

Finally, to solve for T_c (and μ_\uparrow), we need to simplify the expressions for the dispersion of the pairs. Defining $\sum_{\mathbf{k}} f(\xi_{\mathbf{k}}^\uparrow) \equiv \frac{mt}{\pi^2 d} I_2$, then the coefficient a_0 is given by

$$\begin{aligned} n_p &= a_0 \Delta^2 = \frac{n}{2} - \frac{1}{2} \sum_{\mathbf{k}} f(E_{\mathbf{k}}^\uparrow) + \frac{1}{2} \sum_{\mathbf{k}} [f(E_{\mathbf{k}}^\uparrow) - f(\xi_{\mathbf{k}}^\uparrow)] \\ &= n_\downarrow - \frac{mt}{2\pi^2 d} (I_2 - I_1). \end{aligned} \quad (15)$$

Note here both the integrals I_1 and I_2 depend only on μ_\uparrow and T , which are independent of the pairing strength in the BEC limit. Both will vanish when $p = 0$. However, in the presence of population imbalance, $I_2 - I_1$ will not vanish in the BEC limit due to Eq. (11). Therefore, the pair density, n_p , will approach a constant BEC asymptote, which is smaller than n_\downarrow for $p > 0$. Namely, *not* all minority fermions will be paired up.

The coefficient a_1 is now given by

$$a_1 \Delta^2 = \frac{m^2 t}{8\pi^3 d^2 n_\downarrow} (I_2 - I_1) + \frac{1}{4|\mu|} \left(n_\downarrow + \frac{m^2 t^2}{\pi^3 d^2 n_\downarrow} I_3 \right), \quad (16)$$

where the integral $I_3 = \frac{\pi^2 d}{2m^2} \sum_{\mathbf{k}} \epsilon_{\mathbf{k}} [f(\xi_{\mathbf{k}}^\uparrow) - f(E_{\mathbf{k}}^\uparrow)]$. Again, for $p = 0$, all the I 's vanish, so that Eq. (16) recovers the $p = 0$ result, $a_1 \Delta^2 = n/8|\mu|$. It is a dramatic difference that a finite population imbalance contributes a finite, constant, first term on the right-hand side of Eq. (16).

After some lengthy but straightforward derivation, we obtain

$$B_{\parallel} = \frac{1}{4m} + \frac{1}{4n_p} \left[\frac{t}{2\pi^2 d} (3I_2 + I_1) - \frac{m^2 t^2}{2\pi^3 d^2 n_\downarrow} I_4 \right], \quad (17)$$

where $I_4 = \frac{\pi^2 d}{2m^2 t^2} \sum_{\mathbf{k}} [f(\xi_{\mathbf{k}}^\uparrow) - f(E_{\mathbf{k}}^\uparrow)] k_{\parallel}^2$. The first term is the $p = 0$ result, while the rest is the contribution of population imbalance. Here we have kept only the leading-order terms and dropped terms of order $1/\mu$ or higher. The pair density n_p is to be replaced with Eq. (15).

The pair hopping integral t_B is given by

$$\begin{aligned} t_B &= \frac{t^2}{n_p} \left\{ \frac{m}{2\pi^2 d} \left(I_5 - I_6 + I_7 - \frac{mt}{\pi d n_\downarrow} I_8 \right) \right. \\ &\quad \left. + \frac{n_\downarrow}{2|\mu|} \left(1 - \frac{8}{\pi} I_5 - \frac{4t^2 m^2}{\pi^3 d^2 n_\downarrow^2} I_9 \right) \right\}, \end{aligned} \quad (18)$$

where

$$I_5 = \frac{\pi^2 d}{mt} \sum_{\mathbf{k}} f(E_{\mathbf{k}}^\uparrow) \cos(k_z d),$$

$$I_6 = \frac{\pi^2 d}{mt} \sum_{\mathbf{k}} f(\xi_{\mathbf{k}}^\uparrow) \cos(k_z d),$$

$$I_7 = -\frac{4\pi^2 d}{m} \sum_{\mathbf{k}} f'(\xi_{\mathbf{k}}^\uparrow) \sin^2(k_z d),$$

$$I_8 = \frac{\pi^2 d}{mt} \sum_{\mathbf{k}} [f(\xi_{\mathbf{k}}^\uparrow) - f(E_{\mathbf{k}}^\uparrow)] \sin^2(k_z d),$$

$$I_9 = \frac{\pi^2 d}{2mt^2} \sum_{\mathbf{k}} \epsilon_{\mathbf{k}} [f(\xi_{\mathbf{k}}^\uparrow) - f(E_{\mathbf{k}}^\uparrow)] \sin^2(k_z d).$$

For $p = 0$, all integral I 's vanish so that Eq. (18) reduces to the $p = 0$ result, $t_B = t^2/2|\mu|$. As in Eq. (17), here n_p is to be replaced with Eq. (15). Once again, population imbalance leads to the first term in the brackets in Eq. (18), which is a constant of interaction strength and thus becomes the dominant term. This will dramatically change the behavior of the T_c solution.

Equation (14) completely determines μ , and then Eq. (10) is used to fully fix the gap Δ , for given $1/k_F a$ in the deep BEC regime. Since the quantities n_p , a_1 , B_{\parallel} , and t_B rely only on μ_\uparrow and T (with corrections of order $O(1/\mu)$), then μ_\uparrow and T_c can be obtained via solving the pseudogap Eq. (5) along with the number difference Eq. (12), with $\Delta_{pg} = \Delta$. Note that Eq. (5) depends only on the product $a_0 \Delta^2$ and the ratio a_0/a_1 but not on the value of Δ . The fact that the leading terms of $a_0 \Delta^2$, $a_1 \Delta^2$, a_0/a_1 , B_{\parallel} , and t_B are all independent of μ or Δ in the presence of a population imbalance implies that μ_\uparrow and T_c , along with these quantities, all approach their respective interaction-independent BEC asymptotes, which depend only on (t, d, p) .

III. NUMERICAL RESULTS AND DISCUSSIONS

In this subsection, we present our results in the presence of a population imbalance, while the parameters $(t, d, 1/k_F a)$ vary.

For our numerical calculations, we define Fermi momentum $k_F = (3\pi^2 n)^{1/3}$ and Fermi energy $E_F \equiv k_B T_F = \hbar^2 k_F^2 / 2m$, as given by a homogeneous, balanced, noninteracting Fermi gas with the same total number density n in 3D.

A. Effect of population imbalance on BCS-BEC crossover

1. An unphysical nearly isotropic case: $t/E_F = 1$ and $k_F d = 1$

First, we consider the case $t/E_F = 1$ and $k_F d = 1$, which is not physically accessible but provides a nearly spherical Fermi surface in the noninteracting limit [32] and thus may serve to

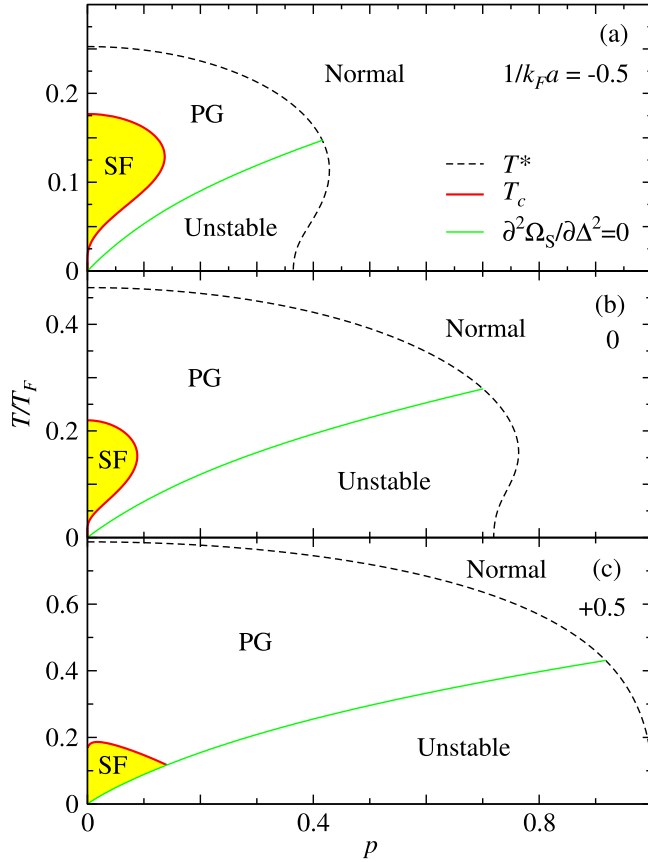


FIG. 1. Evolution of the phase diagram in the $T-p$ plane with $(t/E_F, k_F d) = (1, 1)$, for (a) $1/k_F a = -0.5$, (b) 0, and (c) 0.5, corresponding to near-BCS, unitary, and near-BEC cases, respectively. Here “PG” and “SF” indicate the pseudogapped normal state and superfluid, respectively. The stability condition of Eq. (7) is violated in the “Unstable” region.

make contact with the 3D homogeneous case [26]. Indeed, the result is fairly closed to the 3D homogeneous case, except now there is a weak lattice effect. Nevertheless, it can already be seen that T_c for $p \neq 0$ stops decreasing with pairing strength in the deep BEC regime and thus may become higher than its $p = 0$ counterpart value.

Shown in Fig. 1 is the evolution of the phase diagram in the $T-p$ plane for three representative pairing strengths in the (a) near-BCS, (b) unitary, and (c) near-BEC regimes, respectively. This black dashed line, T^* , was obtained, as an approximation, by solving the mean-field equations with $\Delta = 0$. The phase diagram in each case consists of a small intermediate temperature, Sarma (i.e., polarized) superfluid phase (yellow shaded, labeled “SF”), a large pseudogapped normal phase (“PG”), an unpaired normal Fermi gas phase (“Normal”), as well as an unstable phase (“Unstable”), which often gives way to phase separation. (Note that it is a crossover rather than a true phase transition from the normal to the pseudogapped phases). Solution of possible FFLO states [14,15] have also been contemplated in the “Unstable” region of the phase diagram [25,33–35]. However, the FFLO states are known to be mostly unstable [36], which we shall not consider in the current work. Considering the different vertical

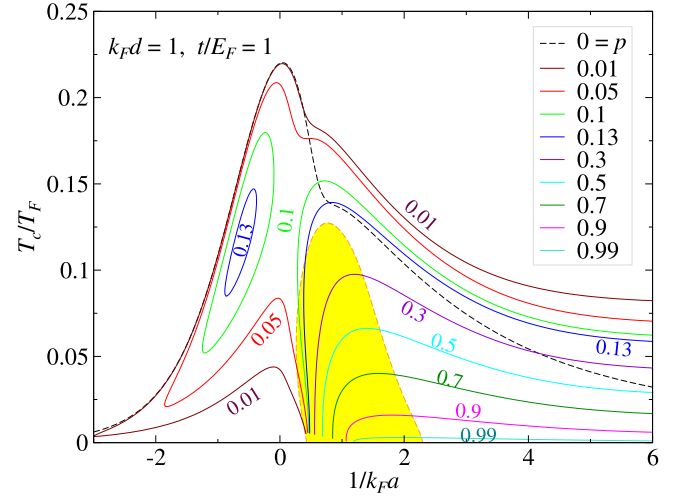


FIG. 2. $T_c-1/k_F a$ phase diagram for different p , as labeled, at fixed $k_F d = 1$ and $t/E_F = 1$. The T_c solutions inside the shaded region are unstable.

scales, the superfluid phase has roughly comparable phase space volumes for the three cases, more or less similar to its homogeneous counterpart in 3D free space, as shown in Figs. 6 and 7 in Ref. [26]. Here the (in)stability condition (green line, separating the Unstable from the PG and the SF phases) is given by Eq. (7). Indeed, For $k_F d = 1$, we have $\pi/d \gg k_F$, so that the confinement in k_z has only a minor impact on the momentum distribution. In addition, similar to the 3D homogeneous situation, the unitary case has the highest T_c at $p = 0$ among all three cases, and there exists no stable Sarma superfluid at $T = 0$ when $p \neq 0$ for the cases considered ($1/k_F a \leq 0.5$). It is worth pointing out that, as shown in Figs. 1(a) and 1(b), approaching $p = 0^+$ along the (red) T_c curve does not end up with a superfluid solution at $T = 0$. This is not an artifact but rather reflects the fact that at $T = 0$, the $p = 0$ and $p \neq 0$ cases are *not* continuously connected in the BCS and unitary regimes. A zero T polarized superfluid solution exists only in the deep BEC regime [23,26]. At the same time, the (red) T_c curve intersects with the (green) instability boundary for the near-BEC case. And in the deep BEC regime, the instability line intersects with the p axis at a finite value, indicating the existence of a stable zero T polarized Sarma superfluid.

Now we turn to the effect of population imbalance on the behavior of T_c throughout the BCS-BEC crossover. Keeping T_c as the function, there are still four independent control variables, p , $1/k_F a$, t and d , which can yield many different facets of the very rich phase space. In this section, we shall only present a few very informative phase diagrams.

Shown in Fig. 2 is the calculated $T_c-1/k_F a$ phase diagram for different p from 0.01 to 0.99 at fixed $k_F d = 1$ and $t/E_F = 1$. For comparison, we also plot the $p = 0$ curve (black dashed). This figure bears a lot of similarity with that for the simple 3D homogeneous case, shown in Ref. [23]. For both cases, there exist intermediate temperature superfluids from the BCS to the near-BEC regime. This unusual phase has a higher and a lower T_c for a given $1/k_F a$. At the same time, for intermediate levels of p (0.1 and 0.13 shown here), the T_c

curve splits into two branches, and the left branch shrinks to zero and disappears as p further increases. The T_c solutions inside the yellow shaded region do not satisfy the stability condition of Eq. (7), and hence are unstable. The difference comes mainly on the BEC side. As $1/k_F a$ increases into the BEC regime, for our present case, T_c decreases, which is qualitatively consistent with the $p = 0$ cases shown in Figs. 1 and 2 in Part I of this work [19], reflecting the lattice effect on pair hopping.

The most surprising feature in Fig. 2 is that T_c for $p = 0$ decreases faster, and thus intersects with the $p \neq 0$ curves. This means that we can get a higher T_c by allowing a small population imbalance on the BEC side of the Feshbach resonance. Indeed, as we have shown analytically in Eq. (18), due to population imbalance, an additional mechanism for pair hopping kicks in; a pair can hop to its neighboring site via exchanging only the majority fermion component of a pair with an excessive majority fermion that is already present on the neighboring site, leaving the previous majority fermion component behind. In this way, the minority fermion component glides through the sites whereas the majority fermions do not necessarily have to hop. Note here that a “site” in the lattice dimension corresponds actually to a 2D plane, which guarantees that, in the thermodynamic limit, there are always excessive majority fermions available on the neighboring “site,” when $p \neq 0$. This is a consequence of lattice-continuum dimensional mixing. The presence of a transverse continuum dimension is crucial for this to happen. Due to this new pair hopping mechanism, t_B approaches a constant in the BEC limit, and so does T_c . Indeed, as one can see, the T_c curves already flatten out toward BEC.

2. Realistic cases with smaller $2mt d^2 < 1$

Now we consider more realistic cases which are accessible experimentally, as constrained by the condition $2mt d^2 < 1$. We show that the superfluid solution may be readily destroyed when t is small. Further varying d may change the topology of the Fermi surface, and thus leads to different behaviors of T_c , especially for the lower branch as to whether a zero temperature superfluid exists at all. When the BEC superfluid exists, the enhancement of T_c due to population imbalance becomes even more pronounced.

Shown in Fig. 3 are the $T-p$ phase diagrams with $(t/E_F, k_F d) = (0.05, 2)$, for the same values of $1/k_F a$ as in Fig. 1. In comparison, we observe that the reduced (t, d) or td^2 has led to significant reduction on T_c and the phase space volumes of the superfluid (“SF”) and paired (“PG” and “Unstable”) phases. This reduction reveals that the small td^2 and relatively large d are detrimental to both superfluidity and pairing. The most dramatic effect is the rapid shrink of the SF phase as $1/k_F a$ increases toward the BEC regime. Furthermore, the T_c curve no longer intersects with the instability line. This suggests that for finite $p > 0$, there is *no* superfluidity at $T = 0$ even in the deep BEC regime, for the present choice of (t, d) . At the same time, the superfluid solution for $p = 0$ always exists [19]; in that case, the area of the SF phase does not completely vanish even though it may become very small. Here one may also notice that the unitary case no longer has the highest T_c . This is because the maximum T_c for $k_F d = 2$

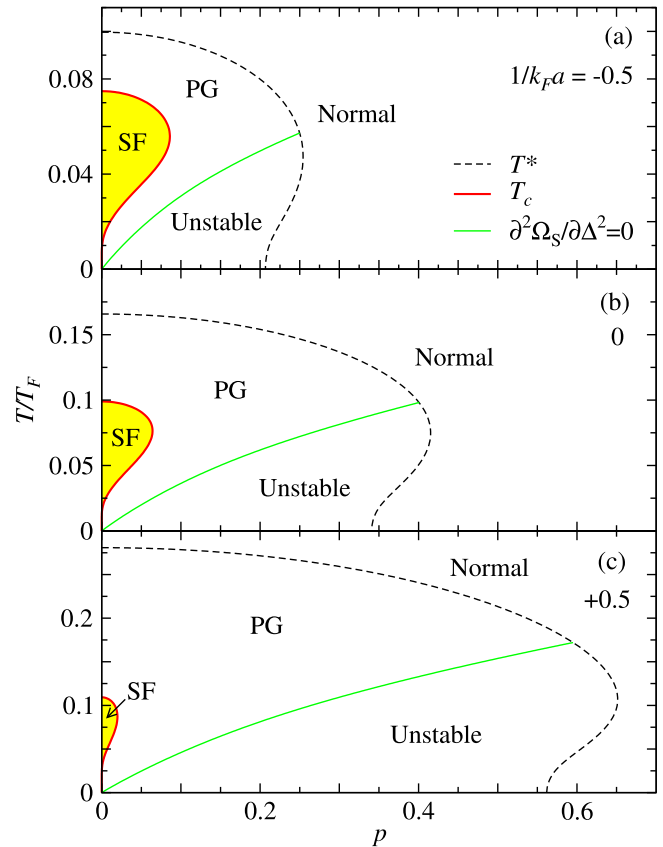


FIG. 3. Evolution of the $T-p$ phase diagram with $t/E_F = 0.05$ and $k_F d = 2$ for different pairing strengths. Other parameters are the same as described in the caption of Fig. 1.

has shifted away from unitarity toward the BEC side in the 1D optical lattice [19]. As one can expect, the smaller t and larger d make the system quasi-2D, giving rise to stronger pairing fluctuations and thus reduced T_c .

In analogy to Fig. 2, we show in Fig. 4 a realistic case with $t/E_F = 0.1$ and $k_F d = 0.5$. With this reduced t and d , the Fermi surface is an elongated ellipsoid in the noninteracting limit, as shown in the inset. Plotted here is T_c as a function of $1/k_F a$ for different p from 0 to 0.132, as labeled next to the color coded curves. Also labeled on the top axis is the effective parameter $1/k_F a_{\text{eff}} = \sqrt{2mt}d/k_F a$, as defined in Part I of this work [19] and Ref. [37]. This parameter is certainly closer to the $1/k_F a$ parameter of the 3D homogeneous case [23]. Similar to that in Fig. 2, the superfluid T_c solution within the small yellow shaded area is unstable. In addition, the lower branch T_c vanishes somewhere close to but on the BEC side of unitarity. In comparison with Fig. 2, however, the overall T_c is strongly suppressed by a factor of 4. This reduced T_c is mainly caused by the small t and small d , which brings the noninteracting chemical potential down dramatically to $\mu \approx 0.276E_F \approx E_F/4$. The other main difference is that the population imbalance p cannot go to a high value as it does in Fig. 2, before T_c disappears completely. While the T_c curve can still persist into the BEC limit for $p \leq 0.1$, it bends back for $p = 0.115$ and forms a superfluid dome in the near-BEC regime. The superfluid phase quickly shrinks when p increases further, and then disappears for $p \gtrsim 0.132$.

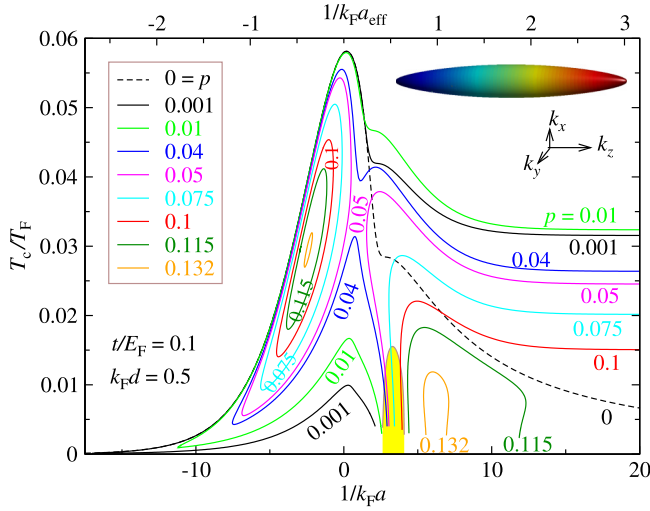


FIG. 4. $T_c - 1/k_F a$ phase diagram for different p from 0 to 0.132 (as labeled) at fixed $k_F d = 0.5$ and $t/E_F = 0.1$, showing dramatic effect of t and d , when compared with Fig. 2. The T_c solution within the yellow shaded area is unstable. Also labeled on the top axis is the effective parameter $1/k_F a_{\text{eff}}$. Shown in the inset is a 3D plot of the Fermi ellipsoid.

To understand the difference between Figs. 2 and 4, we note that the elliptical Fermi surface in Fig. 4 can be rescaled more or less into a sphere; this allows for some similarities in the T_c curves. However, as pairing strength increases and the pairing gap becomes large, the pair occupation number $v_{\mathbf{k}}^2$ (and hence the fermion momentum distribution) will soon feel the confinement of the limited momentum space in the

lattice direction. As a consequence, the excessive majority fermions will no longer be evenly distributed in all directions (after the rescaling). This causes pairing more difficult in the BEC regime and thus leads to a dome shape of the superfluid phase. It also explains why p cannot become large before superfluidity disappears.

Next, we keep $t/E_F = 0.1$ but increase the lattice spacing d to $k_F d = 1.5$ so that the pairs feel more strongly the restriction of $|k_z| \leq \pi/d$. Shown in Fig. 5 are the behaviors of (a, e) T_c , the coefficients (b) B_{\parallel} and (c) B_z , and (d, f) the pair fraction n_p/n_{\downarrow} (all at T_c) as a function of $1/k_F a$ for a series of p from 0 to 0.1. The Fermi surface now has open ends at $k_z = \pm\pi/d$, as shown in the inset of Fig. 5(b). It can no longer become nearly spherical by momentum rescaling. This inevitably shall lead to a bigger difference from Fig. 2. The curves in Figs. 5(a)–5(d) are plotted in a semilog scale, making the exponential dependence of T_c on $1/k_F a$ for $p = 0$ in the BCS regime self-evident as a straight line (orange dashed). It turns out that the coefficients B_{\parallel} , B_z and pair density n_p all bear similar exponential dependencies. Figures 5(e) and 5(f) are plotted in linear scales. In the presence of a finite imbalance p , as the interaction strength *decreases*, T_c follows the $p = 0$ curve until it hits the lower threshold, at which it curves back into a lower branch of T_c . Similar behaviors happen to B_{\parallel} , B_z , and n_p as well. At the same time, on the BEC side of the Feshbach resonance, B_z approaches a constant for $p \neq 0$, (and B_{\parallel} differs substantially from its $p = 0$ value). Accordingly, T_c approaches a constant BEC asymptote, and so does n_p . All superfluid solutions in Fig. 5 are stable. Figures 5(d) and 5(f) reveal that the pair density n_p is higher along the lower branch of T_c than the upper branch, as expected. We note that $n_p/n_{\downarrow} < 1$, indicating that not all minority fermions form

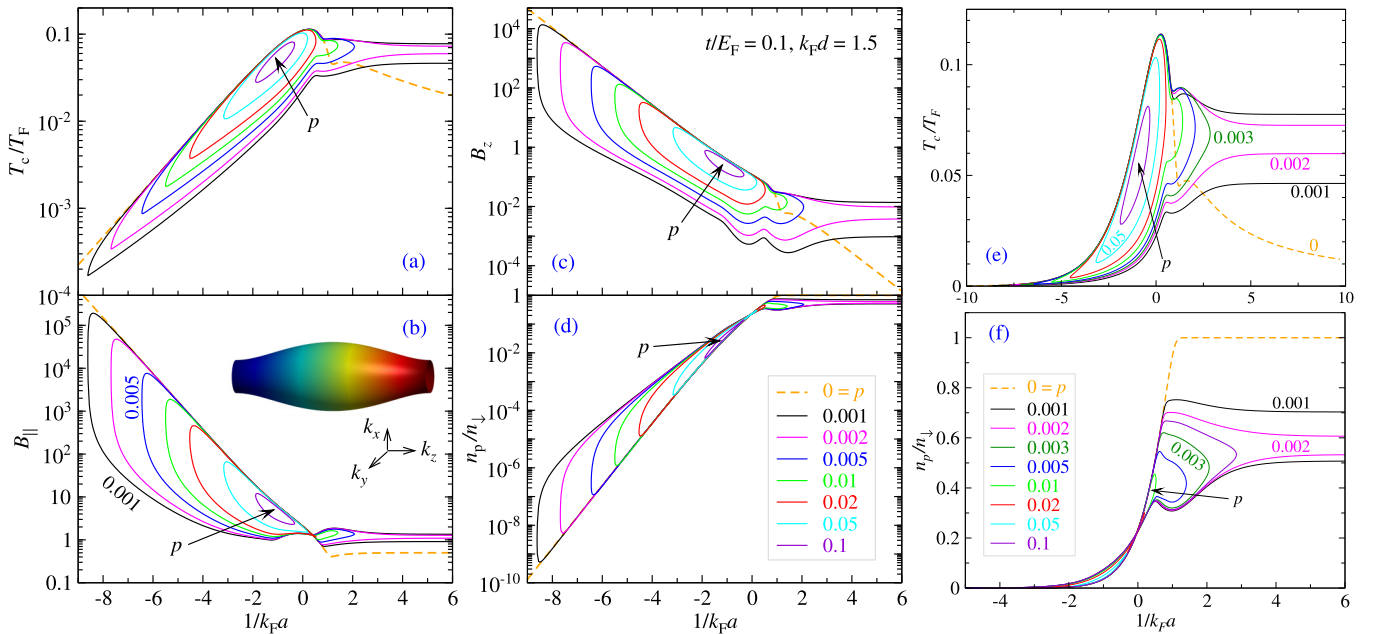


FIG. 5. Behavior of (a, e) T_c/T_F , (b) B_{\parallel} , (c) B_z (in units of $1/2m$) and (d, f) n_p/n_{\downarrow} as a function of $1/k_F a$ for different p from 0 to 0.1 at fixed $k_F d = 1.5$ and $t/E_F = 0.1$. The arrows point to the direction of increasing imbalance p . All panels share the same legend, except (e) and (f) contain an extra $p = 0.003$ line. The lines for $p \geq 0.02$ in panel (f) are barely visible. The inset of panel (b) shows the shape of the Fermi surface.

pairs even in the deepest BEC limit, in contrast to the 3D continuum case. The BEC asymptotic behaviors are governed by Eqs. (15)–(18).

Similar to Fig. 2, in both Figs. 4 and 5 the $p = 0$ curve for T_c quickly drops with increasing $1/k_F a$ and intersects with the $p \neq 0$ curves. Namely, in these physically accessible cases, our earlier finding about the enhancement of T_c by population imbalance remains valid, and the enhancement becomes even more pronounced.

In comparison with Fig. 2, a big qualitative difference is that there is no moderate level of p in Fig. 5 such that the T_c curve splits into a left and a right branch. In addition, due to the big difference between Fermi surfaces of these two cases, the lower T_c here does not vanish in the neighborhood of unitarity, but rather either extends all the way to the BEC limit (for small $p \leq 0.002$) or curls up and joins the upper T_c before it enters the deep BEC regime (for $p \geq 0.003$). The T_c curve for $p = 0.003$ can extend into the BEC regime up to $1/k_F a = 2.854$ or $1/k_F a_{\text{eff}} = 1.354$. Furthermore, here we do not find the counterpart T_c curve that is similar to the $t/E_F = 0.115$ case in Fig. 4. Therefore, while one may find a BEC superfluid for large p up to nearly unity in Fig. 2, it is not possible for the quasi-2D case in Fig. 5. Indeed, the superfluid solution will disappear from the entire phase space when $p > 0.124$ for the present parameters ($t/E_F, k_F d$) = (0.1, 1.5). In other words, superfluidity now exists only in a small portion of the phase space; for small t and relatively not so small d , the superfluid phase can be easily destroyed by a small amount of population imbalance. In addition, a deep BEC superfluid exists only for very low p as well. Reducing t and/or increasing d further may destroy completely the superfluid phase even in the deepest BEC limit. Therefore, one needs to reduce d and/or increase t to have a superfluid with a relatively large p , as will be shown soon below.

We notice that the enhancement of T_c or superfluidity by population imbalance occurs mainly on the BEC side of unitarity. To show this more explicitly, we plot in Fig. 6 the behavior of T_c as a function of p at a series of pairing strengths for fixed ($t/E_F, k_F d$) = (0.2, 2). While one may find a maximum allowable range of p around $1/k_F a = -0.7$, and a maximum T_c at unitarity, these two cases do not see the enhancement effect, since for both cases, T_c reaches its maximum at $p = 0$. In contrast, for $1/k_F a = 1, 1.5$, and 2, as p increases from 0, T_c experiences an initial rapid jump from its $p = 0$ value to a much higher value at $p > 0$, and then slowly drops down and bends back toward $p = 0$. There exists a significant range of p in which T_c is larger than its $p = 0$ counterpart. The back-bending behavior of T_c versus p is consistent with the intermediate temperature superfluidity with an upper and lower T_c . The much reduced maximum p for these cases demonstrates that a superfluid solution exists only for small p on the BEC side of unitarity for the current (t, d) combination.

B. Influence of t and d on the superfluid phase diagrams

The complete phase diagram is multidimensional due to the multiple tuning parameters. In this subsection, we study the effects of the lattice hopping t and lattice constant d , which control the band width and dispersion of the lattice dimension

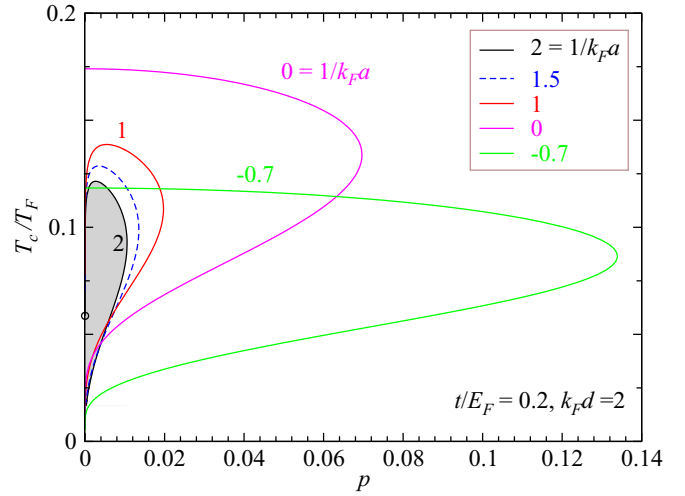


FIG. 6. T_c as a function of p with $k_F d = 2$ for different $1/k_F a$ from -0.7 to 2 at fixed $t/E_F = 0.2$. The intermediate temperature superfluid phase is enclosed within the T_c curve and the vertical axis (shaded for $1/k_F a = 2$). The open circle at $p = 0$ indicates the balanced T_c solution for $1/k_F a = 2$.

as well as the shape and topology of the Fermi surface. We will first present the T_c solutions as a function of p and $1/k_F a$ with different t and d , and then show the continuous evolution of T_c as a function of t and d at fixed p and $1/k_F a$. In this way, we sample the phase space in different directions.

1. $T-p$ and $T-1/k_F a$ phase diagrams for different t and d

In this subsection, we show that the superfluid phase shrinks rapidly as t decreases, and the T_c curve will move toward lower T . In addition, superfluidity in the BEC regime may be destroyed completely for small t . Similarly, for large d , the superfluid phase exists only in the unitary regime.

The effect of increasing t/E_F on the $T-p$ phase diagram is shown in Fig. 7, where T_c versus p at unitarity is plotted for a series of t at $k_F d = 2$. The maximum T_c at $p = 0$ increases

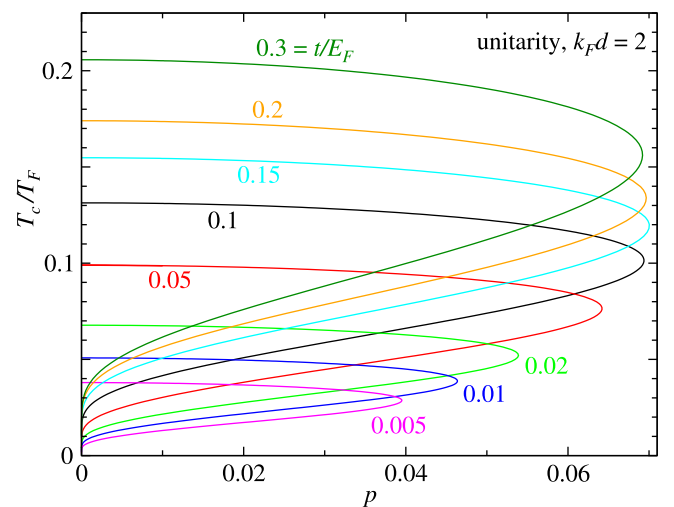


FIG. 7. T_c versus p with $k_F d = 2$ for different values of t/E_F from 0.005 to 0.3 (as labeled) at unitarity.

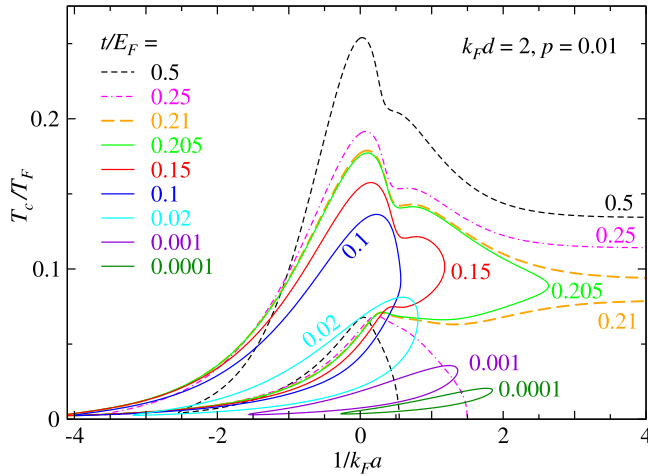


FIG. 8. Behavior of T_c as a function of $1/k_F a$ at fixed $k_F d = 2$ and $p = 0.01$, but for different values of t/E_F , as labeled. It becomes more 3D-like as t increases.

with t , but the maximum reachable p seems to saturate for $t/E_F > 0.1$ for the present choice of $k_F d = 2$.

The evolution of superfluid phase from Figs. 2 to 7 tells that in the presence of a population imbalance, the superfluid phase volume decreases quickly and then disappears completely as the system evolves into the quasi-2D regime.

If we allow ourselves to use somewhat larger range of t , then we will obtain the T_c curves shown in Fig. 8 as a function of $1/k_F a$. Here we fix $p = 0.01$ and $k_F d = 2$, but vary t/E_F from 0.0001 up to 0.5, as labeled. For small $t/E_F \leq 0.1$, we have a simple closed loop. Both T_c and the size of the loop increases as t grows. For $t/E_F = 0.15$ (red) and 0.205 (green curve), the T_c loop extends into the BEC regime, but still cannot reach the deep BEC limit; the T_c curve turns back somewhere on the BEC side of unitarity, and form a closed cycle. As t increases further, for $t/E_F \geq 0.21$, the T_c curves successfully extend all the way into the BEC limit. For $t/E_F = 0.21$ (orange curve), both the upper and lower T_c branches extend to $1/k_F a = +\infty$. However, for $t/E_F \geq 0.25$ (black and pink curves), the lower T_c branch bends downward around unitarity and vanishes at an intermediate pairing strength, somewhere on the BEC side of unitarity. In such a case, there exists a stable homogeneous polarized superfluid in the BEC regime at $T = 0$, similar to the case for a simple 3D continuum. For $k_F d = 2$, our calculation reveals that the Fermi surface has two open ends at $k_z = \pm\pi/d$ for $t/E_F \leq 0.21$, whereas it becomes a closed ellipsoid again for the large $t/E_F \geq 0.25$ cases. The corresponding T_c behavior for the latter cases is similar to that found in Fig. 2.

So far, we have restricted ourselves to fairly small d , with $d \leq 2$. In Fig. 9, we show the behavior of T_c for a large range of d , from $k_F d = 0.1$ to 8, with a fixed $p = 0.01$ and $t/E_F = 0.05$. For $k_F d \geq 4$, we have the range $|k_z| < \pi/d < k_F$, which makes the lattice effect much stronger. Note that for $t/E_F = 0.05$, the $k_F d = 6$ and 8 cases are physically inaccessible. Nonetheless, these curves show a clear trend, namely, with increasing d , the maximum T_c increases and the T_c loop becomes narrower in terms of $1/k_F a$, more concentrated near unitarity. In contrast, for small $k_F d$, π/d becomes very large.

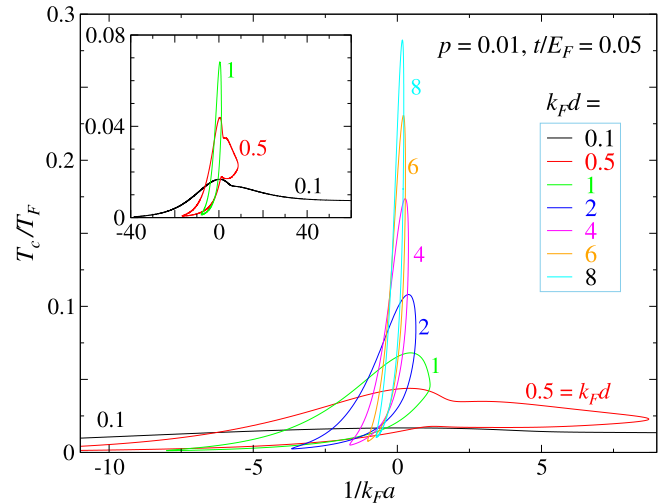


FIG. 9. $T_c - 1/k_F a$ phase diagram for different $k_F d$ from 0.1 to 8 (as labeled) at fixed $p = 0.01$ and $t/E_F = 0.05$. The inset shows the small d cases, which shares the same axis labels as the main figure. Increasing d destroys the superfluid in the deep BEC regime.

With a small t (shown in the inset), the lattice band will be fully occupied, giving rise to an elongated open-end Fermi cylinder (for $k_F d \geq 0.5$) in the momentum space. Due to this small d , except for the $k_F d = 0.1$ case (which has a closed ellipsoid Fermi surface), other T_c curves in the figure cannot access the deep BEC limit. Starting from a small d , this set of curves reveal that increasing d leads to the formation of a closed curve of T_c so that the superfluid phase in the deep BEC regime is destroyed.

From Figs. 2 to 9, we find that the behavior T_c has a close connection to the topology of the Fermi surface. For a closed Fermi surface, it can be brought into a nearly spherical shape by momentum rescaling. For small p , the situation for pairing is very much like in the 3D homogeneous case. Therefore, the T_c curve for low p is similar to its 3D homogeneous counterpart; the lower T_c vanishes in the near BEC regime, and there exists a superfluid ground state in the BEC regime. For open Fermi surfaces, pairing and superfluidity become more difficult, making a ground state superfluid impossible. Note that for a simple tight-binding band in the lattice dimension with nearest-neighbor approximation, the Fermi surface topology changes from closed below half filling to open above half filling. Above half filling, the fermion motion on the Fermi surface becomes more holelike in the k_z direction. While the in-plane motion is always particlelike, this change of character may have detrimental effect on pairing and superfluidity.

2. Continuous evolution of the superfluid phase with t and d

In this subsection, we will sample the multidimensional phase diagram along the t and d directions at fixed p and $1/k_F a$. We find that on the BEC side of unitarity, the lower T_c branch will disappear for large t , so that a BEC superfluid may be found in the ground state. The evolution of the superfluid phase with t and d exhibits strong nonmonotonicity. The T_c curve may split into two disconnected parts as a function of t for moderate d in the BEC regime.

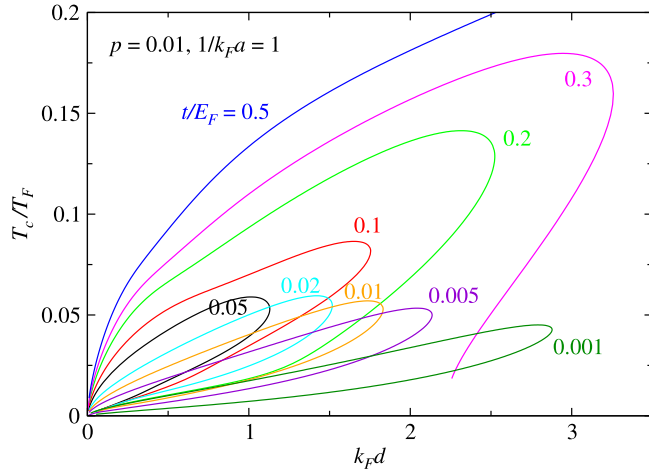


FIG. 10. T_c - d phase diagram for different t/E_F from 0.001 to 0.5, as labeled, at fixed $p = 0.01$ and $1/k_F a = 1$. T_c and the superfluid region both increase as t increases.

Now, we first present how T_c evolves continuously with lattice spacing d . Plotted in Fig. 10 are a series of T_c curves as a function of $k_F d$, for fixed $p = 0.01$ and $1/k_F a = 1$ but different t/E_F from 0.001 to 0.5. Except for the large t/E_F (≥ 0.3) cases, which are unphysical or hard to realize experimentally, T_c curves form a series of loops. This agrees with the existence of two branches at this interaction strength. The superfluid phase space area shrinks with decreasing t . This means that, for small t at the particular $1/k_F a = 1$, a large d will not be able to maintain the superfluid phase. At this pairing strength, the largest reachable value of $k_F d$ is highly nonmonotonic as a function of t , with a minimum of 1.13 for $t/E_F = 0.05$. This also confirms that the ground state at $1/k_F a = 1$ is not a superfluid for $t/E_F \leq 0.2$ and $p = 0.01$. For larger t , the interaction parameter $1/k_F a$ at which the lower T_c would vanish becomes smaller than 1, as can be seen from Fig. 8. This explains why for $t/E_F = 0.3$ and 0.5 in Fig. 10, there is no longer a lower T_c solution for $k_F d \lesssim 2.2$ and 4.1, respectively.

The evolution of T_c with continuously varying t is presented in Fig. 11, for a series of interaction parameter $1/k_F a$ from 0 at unitarity to 7.0 in the BEC regime. Here $p = 0.01$ and $k_F d = 1$ are fixed. Logarithmic and linear scales are used for the horizontal axis in the main figure and the inset, respectively. The log scale serves to magnify the small t regime. For $1/k_F a \leq 1.1$, the curves have an upper and a lower branch, which joins at the small t end. Indeed, from Figs. 1–8, we find that no matter whether the Fermi surface is closed or open, there are always two T_c branches in the unitary and BCS regimes. For $1/k_F a \geq 1.2$, we find that the T_c curves pinch together and then split into two parts around $t/E_F = 0.04$. The left part forms a loop, which shrinks quickly as $1/k_F a$ moves toward BEC. This left loop is the same superfluid phase as the left loop in Fig. 4; they are just different cuts of the superfluid region in the multidimensional phase diagram. For stronger interactions in the BEC regime, either a large t or a very tiny t is needed to maintain a superfluid phase. While the former case allows a closed Fermi surface and thus a superfluid solution in the BEC regime, the latter case will

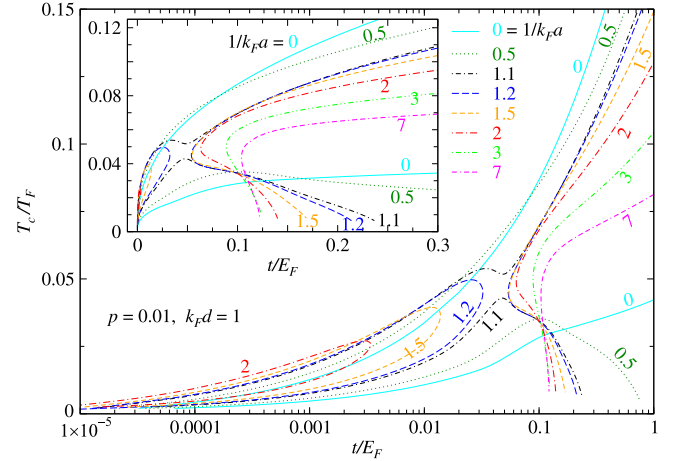


FIG. 11. Behavior of T_c as a function of t/E_F at $p = 0.01$ and $k_F d = 1$, but for different values of $1/k_F a$, as labeled. The inset and the main figure share the same color coding but with different scales for the horizontal axis. The T_c curve splits into two parts when $1/k_F a \geq 1.2$.

allow two branches of T_c which persist into the BEC regime. One can also tell from this figure that, for small $t/E_F < 0.12$, either there is no T_c at all or there is a lower $T_c > 0$, so that the ground state (with $p = 0.01$ and $k_F d = 1$) is *not* a superfluid for $1/k_F a \leq 7$.

Due to the high complexity of the multidimensional phase diagram, the counterpart of the above figures would look somewhat different when $(t, d, p, 1/k_F a)$ changes.

C. Gaps in the superfluid phase

In this subsection, we will present the behavior of various gaps in the superfluid phase. The temperature dependence of the order parameter and the pseudogap can be very nontrivial and different from the balanced case. For the latter case, both are monotonic: the order parameter decreases whereas the pseudogap increases with T at $T \leq T_c$. For an intermediate temperature superfluid, the order parameter Δ_{sc} necessarily vanishes at both the lower and the upper T_c , and thus both Δ_{sc} and the pseudogap Δ_{pg} are nonmonotonic in T .

In Fig. 12, we present, as an example for intermediate temperature superfluidity, the behavior of the order parameter Δ_{sc} , the pseudogap Δ_{pg} and the total gap Δ and a few relevant quantities as a function of temperature in the superfluid phase. Also plotted is the solution above the upper T_c , especially for the pair chemical potential μ_p . Shown in the figure is for the case of $k_F d = 2$, $t/E_F = 0.2$ and $p = 0.01$ at unitarity. It is close to the case of $t/E_F = 0.205$ in Fig. 8. Near the upper T_c , the behavior of the gaps look similar to regular superfluid Fermi gases in the pseudogap regime; The order parameter Δ_{sc} turns on with decreasing T , while the pseudogap Δ_{pg} starts to decrease, leaving the total gap roughly constant or slightly increasing. Above the upper T_c , the pair chemical potential μ_p starts to decrease from 0 with increasing T . The vanishing of Δ_{sc} at the upper T_c is the same as in BEC of ideal Bose gases. As the temperature decreases toward the lower $T_{c,L}$, Δ_{pg} increases again, which suppresses Δ_{sc} quickly down to zero. This can be understood from the highly decreased

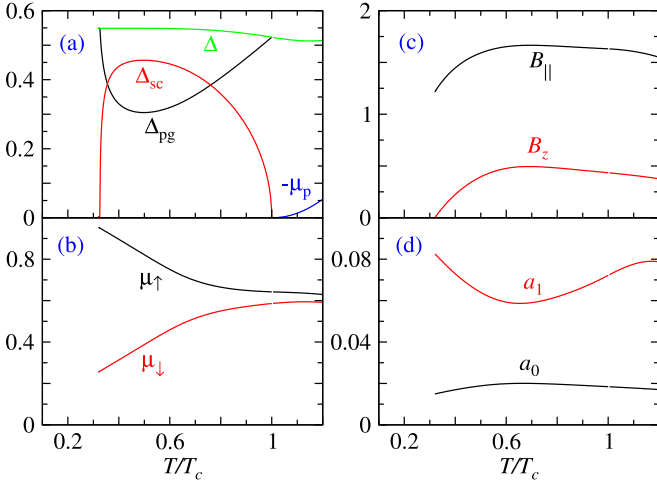


FIG. 12. Behavior of (a) the gaps and μ_p , (b) μ_σ , (c) B_\parallel and B_z , and (d) a_0 and a_1 , as a function of T/T_c , for $t/E_F = 0.2$, $k_F d = 2$ and $p = 0.01$ at unitarity. Here $T_c/T_F = 0.1736$ is the upper T_c , and the lower T_c is $T_{c,L}/T_F = 0.05656$. Gaps and chemical potentials are in units of E_F . The coefficients B 's are in units of $1/2m$, a_0 and a_1 in units of k_F^3/E_F^2 and k_F^3/E_F^3 , respectively.

value of $B_z = t_B d^2$ at $T_{c,L}$ in panel (c); As B_z decreases, pairs become heavy in the lattice direction, leading to reduced energy cost for exciting finite momentum pairs and hence an rapid increase in Δ_{pg} , which then exhausts the order parameter via $\Delta_{sc}^2 = \Delta^2 - \Delta_{pg}^2$. We note that there are no other sharp changes in B_\parallel , a_0 , and a_1 . Further lowering T below $T_{c,L}$ would enter again a normal state. However, the trend of B_z at $T_{c,L}$ suggests that this normal state may soon become unstable against pair density wave (or stripe order) formation in the lattice direction (with a negative B_z at lower T). Other possible solutions in this low T normal state include phase separation and possible FFLO-like solutions with a wavevector along the \hat{z} direction. In fact, the pair density wave solution is similar to an FFLO state, except that it may not exhibit superfluidity. One would need to include the q_z^4 order in the inverse T matrix expansion to obtain a meaningful solution below $T_{c,L}$, which is beyond the scope of current work.

It is interesting to note that while Δ is roughly a constant in T , μ_\uparrow , and μ_\downarrow becomes far apart at low T . This large separation, with $h = 0.346E_F$, is comparable to the Clogston limit for pair breaking [38], $\Delta/\sqrt{2} = 0.388E_F$, where $\Delta/E_F = 0.549$ at $T_{c,L}$. In other words, the disappearance of superfluidity at the lower $T_{c,L}$ is compatible with the Clogston picture as well. The small difference between h and $\Delta/\sqrt{2}$ may be attributable to the deviation of the Fermi surface from an isotropic 3D sphere [39]. In addition, here the gap is large (beyond the BCS regime) so that self-consistent calculations are important. However, at the upper T_c , h is much smaller than $\Delta/\sqrt{2}$, implying that the vanishing of the superfluid order at the upper T_c is not associated with the Clogston picture but rather driven by pairing fluctuations.

D. Superfluid density

In this section, we show the behavior of the superfluid density. Here we choose to show only cases of intermediate

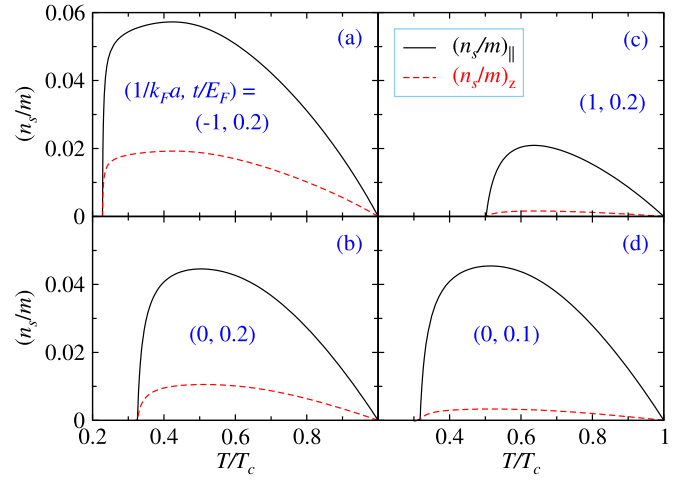


FIG. 13. Behavior of the in-plane (black) and lattice components (red dashed) of the superfluid density (n_s/m) as a function of T/T_c , for $k_F d = 2$, $p = 0.01$, and (a) $(1/k_F a, t/E_F) = (-1, 0.2)$, (b) $(0, 0.2)$, (c) $(1, 0.2)$, and (d) $(0, 0.1)$, with $(T_c/T_F, T_{c,L}/T_F) = (0.0923, 0.0210)$, $(0.1736, 0.0566)$, $(0.1362, 0.0684)$, and $(0.1310, 0.0416)$, respectively. All panels share the same legends.

temperature superfluidity, with both an upper T_c and a lower $T_{c,L}$, as in Sec. III C. Cases without a lower T_c for large t are more qualitatively similar to their balanced counterpart shown in Part I of this work [19].

Plotted in Fig. 13 are the temperature dependence of both the in-plane (black curves) and lattice components (red curves) of (n_s/m) for $k_F d = 2$ with $p = 0.01$. Panels (a–c) are for the BCS, unitary and BEC cases, respectively, for $t/E_F = 0.2$. The corresponding curve of T_c versus $1/k_F a$ is close to the green one for $t/E_F = 0.205$ in Fig. 8. These results suggest that both components decreases as $1/k_F a$ increases. The suppression of the lattice component, $(n_s/m)_z$, can be attributed more to the effect that the system becomes more 2D and t_B decreases with increasing pairing strength. However, the reduction of the in-plane $(n_s/m)_\parallel$ is likely due to the increase of the pseudogap Δ_{pg} with decreasing T toward $T_{c,L}$, leading to premature shut-off of the superfluid density before it fully reaches its maximum possible value (normally) at $T = 0$.

Shown for comparison in Fig. 13(d) is the case of $t/E_F = 0.1$ at unitarity, with other parameters the same as in Fig. 13(b). As can be seen, the in-plane curves are very close to each other for these two cases. However, the lattice component is drastically suppressed by the smaller t in Fig. 13(d). This can be understood qualitatively from the increased fermion band mass and hence the pair mass in the \hat{z} direction.

For all panels in Fig. 13, the temperature dependencies of both components are close to each other, despite their rather different magnitudes. This is because the main T dependence comes from the common prefactor Δ_{sc}^2 in Eq. (8).

E. BEC asymptotic behavior with $p \neq 0$

Finally, in this subsection, we verify numerically our derivations about the asymptotic behavior in the BEC regime

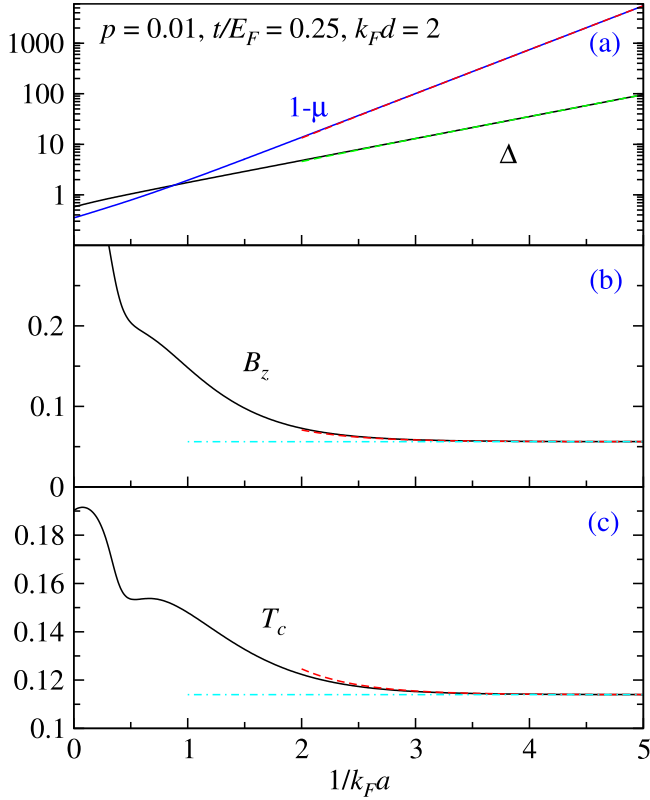


FIG. 14. Behavior of (a) $1 - \mu$ and Δ , (b) B_z , and (c) T_c as a function of $1/k_F a$, and comparison with the asymptotic solutions in the BEC regime. The solid lines are full numerical solution, and the dashed lines are the asymptotic solution, and the (cyan) dot-dashed lines are the BEC asymptote. Here $p = 0.01$, $t/E_F = 0.25$, and $k_F d = 2$.

in Sec. II D. This will confirm our analytical understanding of the physics. It will show that, despite the complicated, and highly unusual behavior of the superfluid phase, it can be largely understood analytically.

Show in Fig. 14 is the asymptotic behavior of μ , Δ , B_z , and T_c in the BEC limit. Plotted in Fig. 14 are $1 - \mu$ and Δ in units of E_F versus $1/k_F a$ in a semilog scale. The straight lines confirm their exponential dependence on $1/k_F a$. The dashed lines are analytical asymptotic solution, in perfect agreement with full numerical solutions (solid lines). The red dashed lines in Figs. 14(b) and 14(c) present the solution obtained using the asymptotic expansions, while the cyan dot-dashed lines represent the deepest BEC asymptotes. Clearly, the asymptotic expansions and the BEC asymptotes are all in quantitative agreement with the full numerical solutions. This provides direct support of our analytical derivations in the BEC regime. These plots demonstrate that in the deep BEC limit, B_z and T_c approach a constant asymptote, as also shown in Fig. 5. Similar constant asymptotic behaviors are found for B_{\parallel} , $a_0 \Delta^2$, and $a_1 \Delta^2$ as well, a plot of which can be seen in Ref. [37].

Given these BEC asymptotic behaviors, we can investigate the phase diagrams in the BEC limit as a function of t , d and p . Shown in Fig. 15(a) is the BEC asymptote of T_c with $t/E_F = 0.1$ as a function of p with different $k_F d = 0.25, 0.5,$

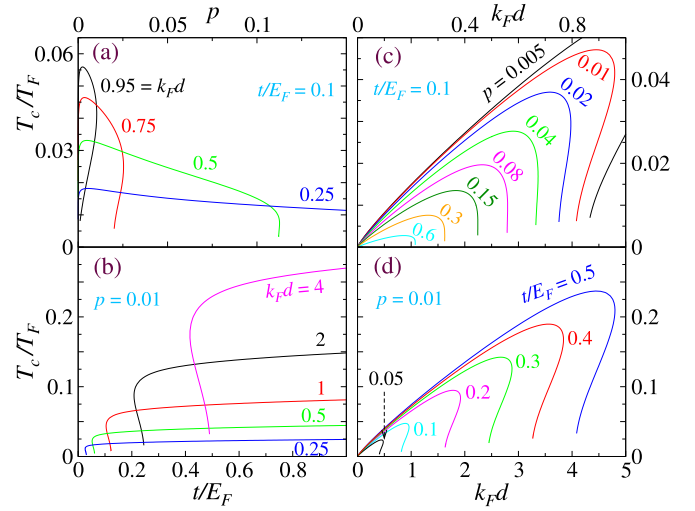


FIG. 15. Behavior of the BEC asymptote of T_c , as a function (a) of p for fixed $t/E_F = 0.1$ with different $k_F d$ from 0.25 to 0.95, (b) of t/E_F for fixed $p = 0.01$ with varying $k_F d$ from 0.25 to 4, (c, d) of $k_F d$ for (c) fixed $t/E_F = 0.1$ with varying p from 0.005 to 0.6 and for, (d) fixed $p = 0.01$ with varying t/E_F from 0.05 to 0.5. The parameters are labeled on the curves.

0.75, and 0.95. The Fermi surface topology at $p = 0$ changes from closed to open, as the lattice spacing increases across $k_F d = 0.942$. Therefore, nearly all cases shown here have a closed Fermi surface. It can be readily seen that for $k_F d = 0.95$, the maximum p is only about 0.01; there is no BEC superfluid solution for larger p . The maximum p increases as d decreases. For smaller $k_F d = 0.25$, p survives up to about 0.475. This may largely have to do with the fact that a smaller d places less restrictive confinement for pair motion in the k_z direction, and thus the system is closer to the 3D case, so that it can accommodate a larger population imbalance.

Plotted in Fig. 15(b) are T_c curves with $p = 0.01$ as a function of t/E_F with different $k_F d = 4, 2, 1, 0.5,$ and down to 0.25. These curves demonstrate that the lowest threshold of t for having a BEC superfluid solution increases with d . For $k_F d = 4$, we need $t/E_F \gtrsim 0.42$. For $k_F d = 2$, the threshold drops to about 0.21, in agreement with Fig. 8. For $k_F d = 0.25$, the threshold becomes $t/E_F \approx 0.03$. In particular, for $k_F d = 1$, the threshold is about 0.105 (> 0.1). This explains why there is no $k_F d = 1$ curve in panel (a), calculated for $t/E_F = 0.1$. As d increases, the overall T_c also increases, since the 2D planar density n_{2D} increases and so does the noninteracting chemical potential. In reality, t is normally small. This requires a small d to have a BEC superfluid, as one can see from Fig. 9 as an example, where only the $k_F d = 0.1$ curve persists into the BEC limit for small $t/E_F = 0.05$. Our calculations show that these thresholds roughly correspond to half filling of the lattice band, where the Fermi surface topology changes.

Presented in Fig. 15(c) is the BEC asymptote of T_c calculated for $t/E_F = 0.1$, as a function of $k_F d$ with different population imbalances from $p = 0.005$ to 0.6. The maximum allowed $k_F d$ decreases quickly with increasing p . For $p = 0.005$, $k_F d$ goes up to 1.2. For $p = 0.01$, $k_F d$ is allowed up to about 0.96. For $p = 0.6$, one needs a small $k_F d < 0.22$ to have a BEC superfluid. Figure 15(c) also reveals that for a

given d , there is a maximum allowed p , beyond which the BEC superfluid solution no longer exists, in agreement with Fig. 15(a).

Shown in Fig. 15(d) is the BEC asymptote of T_c calculated for $p = 0.01$, as a function of $k_F d$ with different tunneling t/E_F from 0.05 to 0.5. As is shown, the maximum possible d increases with t . While for $t/E_F = 0.5$ this maximum is about 4.8, it decreases down to about 0.49 for $t/E_F = 0.05$. If one wants to have a larger d for the same small t , then one will need to use a smaller p , as indicated by Fig. 15(c). The lower end $t/E_F = 0.05$ is more realistic. It means that for a typical $k_F d \sim 1$, a small amount of population imbalance will be sufficient to destroy the superfluid solutions in the BEC regime [40].

We point out that in all four panels of Fig. 15, there exists a narrow range of the parameters where the T_c curve bends back and thus is double-valued, which correspond to the two branches such as the low p curves shown in Fig. 5(e), with an open Fermi surface. For the rest part of the curves, there is only one (upper) T_c , corresponding to, e.g., the low p curves in Fig. 4, with a closed Fermi surface.

F. Further discussions

From the numerical results presented above, we see that the behavior of T_c and the phase diagrams are very complex, in the presence of a population imbalance. In the physically accessible scope of the parameters, e.g., constrained by the condition $2mt d^2 < 1$, the superfluid phase occupies only a very restricted small volume in the multidimensional phase space. Superfluidity can be easily destroyed by small amount of population imbalance when the lattice constant d becomes large and/or the tunneling matrix element t becomes small. To understand this destruction of superfluidity, we notice that large d and small t put the system in the quasi-2D regime, such that the lattice band is essentially fully occupied, and in-plane chemical potential (in the noninteracting limit) is much higher than the lattice band width $2t$, leaving almost no dispersion on the Fermi surface along the lattice direction. Excessive fermions will necessarily have to occupy high in-plane momentum states and thus cost a lot of excitation energy. In this case, a small population imbalance will create a substantial mismatch h in chemical potentials that is sufficient to destroy pairing.

In contrast, we find that smaller d is more benign in the behavior of T_c , e.g., the $k_F d = 0.1$ case in Fig. 9. For small d , the momentum space constraint $|k_z| < \pi/d$ in the lattice direction becomes less restrictive so that the Fermi surface becomes an ellipsoid, which can be mapped back into a sphere via momentum rescaling. Whether closed or open, the Fermi surface topology in the noninteracting limit plays an important role in classifying the behavior of the T_c curves. With a closed Fermi surface, the superfluid solution in the BEC regime (if it exists) has only one (upper) T_c . In contrast, with an open Fermi surface, the superfluid has both an upper and a lower T_c , so that ground state superfluidity is not allowed. Further careful analysis may involve different Fermi surfaces for the two spin components and how their influence evolves with p .

More surprisingly, when the superfluid solution exists in the BEC regime or on the BEC side of unitarity, T_c can

be substantially enhanced by a small amount of population imbalance with respect to the balanced case. Via analytical analysis in the BEC regime, we show that this enhancement is associated with contributions to t_B from excessive unpaired majority atoms. These contributions lead to a constant BEC asymptote for t_B and a few other relevant quantities, and hence a constant BEC asymptote for T_c via the pseudogap equation. These contributions to t_B constitute a new pair hopping mechanism assisted by excessive majority atoms. *For this mechanism to work, it is important that there is at least one transverse continuum dimension.* In the present case of 1D optical lattice, there are two transverse continuum dimensions, i.e., the 2D xy plane. This guarantees that there are always excessive majority atoms available on a neighboring lattice “site.” Therefore, *lattice-continuum mixing is crucial for this unusual behavior.*

Another important difference between 1D optical lattices and the 3D continuum case is the pair fraction in the BEC limit. For the latter case, all minority atoms will form pairs, namely, $n_p/n_\downarrow = 1$ in the BEC limit. In contrast, for the present case, we always have $n_p/n_\downarrow < 1$ for nonzero p , as can be seen from Eq. (15). The difference can be attributed to the quasi-two dimensionality (quasi-2D) in the present case, which leads to a constant ratio of $\Delta^2/|\mu|$ in the BEC limit, in contrast to vanishing as $1/\sqrt{|\mu|}$ in 3D continuum.

As one can see, the most unusual behaviors, in comparison with their 3D continuum counterpart, are observed in the BEC regime. Since they are mostly connected to the topology of the Fermi surface, and the general feature of lattice-continuum mixing (the latter leads to topologically different geometry from the 3D continuum space), we believe that these results are qualitatively stable. Different approximations shall only lead to minor quantitative corrections.

Our calculations are based on the assumption that the 2D planes are homogeneous. In real experiments, they are always finite and confined in a shallow trapping potential. At the same time, the lattice direction is confined by a trapping potential as well. The finite size and trap effects are beyond the scope of the current work and will be left for future investigations. We note that recent progress in implementing uniform box trapping potential [41–43] can greatly reduce the complexity.

One interesting question is to ask when the 1DOL lattice will be reduced to a 2D system such as a tightly confined single pancakelike 2D trap. One may be tempted to think that the latter corresponds the small d limit. However, since the lattice potential is unlike a hard-wall box trap, a small d often means easy tunneling between neighboring lattice sites, and also a large first BZ, which makes the system more 3D like. Therefore, to reach the 2D limit, it is crucial to keep the tunnel matrix element t small. This will keep the lattice dimension fully occupied and nearly dispersionless. Note that the phase space density in the lattice dimension is always 1, as $d(2\pi/d)/(2\pi) = 1$, which can be thought of as the single energy level in the normal direction for the tightly confined 2D trap. Therefore, for given d , the 2D limit is approached when t is so small that the dispersion in the lattice direction is negligible. Behaviors of population imbalanced Fermi gases in 2D have also been under active investigation experimentally [31,44] and theoretically [45–50].

IV. CONCLUSIONS

In summary, we have studied the ultracold atomic Fermi gases in a 1D optical lattice in the presence of population imbalance with a pairing fluctuation theory, as they undergo a BCS-BEC crossover. We find that superfluidity exists only for a very restricted range of parameters, while it can be readily destroyed by a small amount of imbalance p at large d and small t . When the superfluid solution does exist on the BEC side of the Feshbach resonance, T_c can be enhanced substantially by even a tiny amount of population imbalance, via the new pair hopping mechanism assisted by excessive majority atoms. In general, when t is small, the T_c curve bends back on the BEC side and the superfluidity disappears in the deep BEC regime. Meanwhile, the superfluid phase shrinks as p increases. For fixed d and p , the superfluid region in the $T-1/k_F a$ plane shrinks as t decreases, while for fixed p and t , the T_c curve forms a closed loop in the $T-1/k_F a$ plane and becomes narrower near unitarity as d increases. In general, whether there is only one (upper) T_c or there are both an upper and a lower T_c in the BEC regime depends largely on the Fermi surface topology. The former occurs with a closed ellipsoidal Fermi surface, while the latter happens when the Fermi surface has two open ends at the Brillouin zone boundaries. Furthermore, due to the quasi-two dimensionality, only part of the minority atoms will be paired even if superfluidity exists in the BEC limit.

Before a general formula relating the scattering length a with its 3D continuum counterpart a_{3D} is available, one

can use the chemical potential μ as a control variable in experiment.

Our results demonstrate that experimentally one needs to be careful to maintain a good population balance to stay in the superfluid phase. However, a perfect balance may not always be desirable. A small amount of imbalance may be good for enhancing T_c , making the superfluid phase easier to access. It may take some trial and error to find the optimal parameters in experiment.

These predicted behaviors of fermions on a 1D optical lattice are very different from pure 3D continuum or 3D lattices, and have not been reported in the literature. Since optical lattices have been realized experimentally for a long time, these predictions should be tested in future experiments.

ACKNOWLEDGMENTS

We thank Chenchao Xu and Yanming Che for useful discussions. This work was supported by the NSF of China (Grants No. 11774309 and No. 11674283) and the NSF of Zhejiang Province of China (Grant No. LZ13A040001). C.L. was supported by the Key-Area Research and Development Program of Guangdong Province, China under Grant No. 2019B030330001, the NSF of China under Grants No. 11874434 and No. 11574405, and the Science and Technology Program of Guangzhou, Guangdong Province, China under Grant No. 201904020024.

-
- [1] Q. J. Chen, J. Stajic, S. N. Tan, and K. Levin, BCS-BEC crossover: From high temperature superconductors to ultracold superfluids, *Phys. Rep.* **412**, 1 (2005).
 - [2] I. Bloch, J. Dalibard, and W. Zwerger, Many-body physics with ultracold gases, *Rev. Mod. Phys.* **80**, 885 (2008).
 - [3] S. Giorgini, L. P. Pitaevskii, and S. Stringari, Theory of ultracold atomic Fermi gases, *Rev. Mod. Phys.* **80**, 1215 (2008).
 - [4] A. Cichy and R. Micnas, The spin-imbalanced attractive Hubbard model in $d = 3$: Phase diagrams and BCS-BEC crossover at low filling, *Ann. Phys.* **347**, 207 (2014).
 - [5] P. Dyke, E. D. Kuhnle, S. Whitlock, H. Hu, M. Mark, S. Hoinka, M. Lingham, P. Hannaford, and C. J. Vale, Crossover from 2D to 3D in a Weakly Interacting Fermi Gas, *Phys. Rev. Lett.* **106**, 105304 (2011).
 - [6] A. T. Sommer, L. W. Cheuk, M. J. H. Ku, W. S. Bakr, and M. W. Zwierlein, Evolution of Fermion Pairing from Three to Two Dimensions, *Phys. Rev. Lett.* **108**, 045302 (2012).
 - [7] M. Feld, B. Froehlich, E. Vogt, M. Koschorreck, and M. Köhl, Observation of a pairing pseudogap in a two-dimensional Fermi gas, *Nature* **480**, 75 (2011).
 - [8] S.-J. Gu, R. Fan, and H.-Q. Lin, Ground state of a mixture of two species of fermionic atoms in a one-dimensional optical lattice, *Phys. Rev. B* **76**, 125107 (2007).
 - [9] A. E. Feiguin and F. Heidrich-Meisner, Pairing states of a polarized Fermi gas trapped in a one-dimensional optical lattice, *Phys. Rev. B* **76**, 220508(R) (2007).
 - [10] M. Rizzi, M. Polini, M. A. Cazalilla, M. R. Bakhtiari, M. P. Tosi, and R. Fazio, Fulde-Ferrell-Larkin-Ovchinnikov superfluidity in one-dimensional optical lattices, *Phys. Rev. B* **77**, 245105 (2008).
 - [11] M. R. Bakhtiari, M. J. Leskinen, and P. Törmä, Spectral Signatures of the Fulde-Ferrell-Larkin-Ovchinnikov Order Parameter in One-Dimensional Optical Lattices, *Phys. Rev. Lett.* **101**, 120404 (2008).
 - [12] T. Roscilde, C. D. E. Boschi, and M. Dalmonte, Pairing, crystallization and string correlations of mass-imbalanced atomic mixtures in one-dimensional optical lattices, *Europhys. Lett.* **97**, 23002 (2012).
 - [13] V. V. Franca, D. Hördlein, and A. Buchleitner, Fulde-Ferrell-Larkin-Ovchinnikov critical polarization in one-dimensional fermionic optical lattices, *Phys. Rev. A* **86**, 033622 (2012).
 - [14] P. Fulde and R. A. Ferrell, Superconductivity in a strong spin-exchange field, *Phys. Rev.* **135**, A550 (1964).
 - [15] A. I. Larkin and Y. N. Ovchinnikov, Inhomogeneous state of superconductors, *Sov. Phys. JETP* **20**, 762 (1965) [*Zh. Eksp. Teor. Fiz.* **47**, 1136 (1964)].
 - [16] J. P. A. Devreese, S. N. Klimin, and J. Tempere, Resonant enhancement of the Fulde-Ferrell-Larkin-Ovchinnikov state in three dimensions by a one-dimensional optical potential, *Phys. Rev. A* **83**, 013606 (2011).
 - [17] J. P. A. Devreese, M. Wouters, and J. Tempere, Controlling the pair momentum of the Fulde-Ferrell-Larkin-Ovchinnikov state in a three-dimensional Fermi gas through a one-dimensional periodic potential, *Phys. Rev. A* **84**, 043623 (2011).
 - [18] J. P. A. Devreese, S. Klimin, M. Wouters, and J. Tempere, The Fulde-Ferrell-Larkin-Ovchinnikov state in a 3D Fermi gas

- subjected to a 1D periodic potential, *Mod. Phys. Lett. B* **26**, 1230014 (2012).
- [19] J. B. Wang, L. F. Zhang, Y. Yu, C. H. Lee, and Q. J. Chen, *Phys. Rev. A* **101**, 053617 (2020).
- [20] P. Nozières and S. Schmitt-Rink, Bose condensation in an attractive fermion gas: From weak to strong coupling superconductivity, *J. Low Temp. Phys.* **59**, 195 (1985).
- [21] Q. J. Chen and J. B. Wang, Pseudogap phenomena in ultracold atomic Fermi gases, *Front. Phys.* **9**, 539 (2014).
- [22] E. J. Mueller, Review of pseudogaps in strongly interacting Fermi gases, *Rep. Prog. Phys.* **80**, 104401 (2017).
- [23] C.-C. Chien, Q. J. Chen, Y. He, and K. Levin, Intermediate Temperature Superfluidity in a Fermi Gas with Population Imbalance, *Phys. Rev. Lett.* **97**, 090402 (2006).
- [24] A. Sedrakian and U. Lombardo, Thermodynamics of a $n - p$ Condensate in Asymmetric Nuclear Matter, *Phys. Rev. Lett.* **84**, 602 (2000).
- [25] L. He, M. Jin, and P. Zhuang, Finite-temperature phase diagram of a two-component Fermi gas with density imbalance, *Phys. Rev. B* **74**, 214516 (2006).
- [26] Q. J. Chen, Y. He, C.-C. Chien, and K. Levin, Stability conditions and phase diagrams for two-component Fermi gases with population imbalance, *Phys. Rev. A* **74**, 063603 (2006).
- [27] G. Sarma, On the influence of a uniform exchange field acting on the spins of the conducting electrons in a superconductor, *J. Phys. Chem. Solids* **24**, 1029 (1963).
- [28] C.-H. Pao, S.-T. Wu, and S.-K. Yip, Superfluid stability in the BEC-BCS crossover, *Phys. Rev. B* **73**, 132506 (2006).
- [29] Q. J. Chen, I. Kosztin, B. Jankó, and K. Levin, Pairing Fluctuation Theory of Superconducting Properties in Underdoped to Overdoped Cuprates, *Phys. Rev. Lett.* **81**, 4708 (1998).
- [30] Y. He, C.-C. Chien, Q. J. Chen, and K. Levin, Thermodynamics and superfluid density in BCS-BEC crossover with and without population imbalance, *Phys. Rev. B* **76**, 224516 (2007).
- [31] W. Ong, C. Cheng, I. Arakelyan, and J. E. Thomas, Spin-Imbalanced Quasi-Two-Dimensional Fermi Gases, *Phys. Rev. Lett.* **114**, 110403 (2015).
- [32] L. F. Zhang, Y. M. Che, J. B. Wang, and Q. J. Chen, Exotic superfluidity and pairing phenomena in atomic Fermi gases in mixed dimensions, *Sci. Rep.* **7**, 12948 (2017).
- [33] Y. He, C.-C. Chien, Q. Chen, and K. Levin, Single-plane-wave Larkin-Ovchinnikov-Fulde-Ferrell state in BCS-BEC crossover, *Phys. Rev. A* **75**, 021602(R) (2007).
- [34] D. E. Sheehy and L. Radzihovsky, Comment on “Superfluid stability in the BEC-BCS crossover,” *Phys. Rev. B* **75**, 136501 (2007).
- [35] J. B. Wang, Y. M. Che, L. F. Zhang, and Q. J. Chen, Enhancement effect of mass imbalance on Fulde-Ferrell-Larkin-Ovchinnikov type of pairing in Fermi-Fermi mixtures of ultracold quantum gases, *Sci. Rep.* **7**, 39783 (2017).
- [36] J. B. Wang, Y. M. Che, L. F. Zhang, and Q. J. Chen, Instability of Fulde-Ferrell-Larkin-Ovchinnikov states in three and two dimensions, *Phys. Rev. B* **97**, 134513 (2018).
- [37] Q. J. Chen, J. B. Wang, L. Sun, and Y. Yu, Unusual destruction and enhancement of superfluidity of atomic Fermi gases by population imbalance in a one-dimensional optical lattice, *Chin. Phys. Lett.* **37**, 053702 (2020).
- [38] A. M. Clogston, Upper Limit for the Critical Field in Hard Superconductors, *Phys. Rev. Lett.* **9**, 266 (1962).
- [39] In principle, here the gap Δ should be the one calculated in the absence of imbalance in the original Clogston derivation. For $p = 0.01$, the gap is close to its $p = 0$ value.
- [40] We note that in Fig. 15 most T_c curves do not extend down to zero T . This happens mainly because B_z becomes exponentially small, causing round-off errors and making it difficult to obtain a precise solution numerically.
- [41] A. L. Gaunt, T. F. Schmidutz, I. Gotlibovych, R. P. Smith, and Z. Hadzibabic, Bose-Einstein Condensation of Atoms in a Uniform Potential, *Phys. Rev. Lett.* **110**, 200406 (2013).
- [42] B. Mukherjee, Z. Yan, P. B. Patel, Z. Hadzibabic, T. Yefsah, J. Struck, and M. W. Zwierlein, Homogeneous Atomic Fermi Gases, *Phys. Rev. Lett.* **118**, 123401 (2017).
- [43] K. Hueck, N. Luick, L. Sobirey, J. Siegl, T. Lompe, and H. Moritz, Two-Dimensional Homogeneous Fermi Gases, *Phys. Rev. Lett.* **120**, 060402 (2018).
- [44] D. Mitra, P. T. Brown, P. Schauß, S. S. Kondov, and W. S. Bakr, Phase Separation and Pair Condensation in a Spin-Imbalanced 2D Fermi Gas, *Phys. Rev. Lett.* **117**, 093601 (2016).
- [45] G. J. Conduit, P. H. Conlon, and B. D. Simons, Superfluidity at the BEC-BCS crossover in two-dimensional Fermi gases with population and mass imbalance, *Phys. Rev. A* **77**, 053617 (2008).
- [46] L. He and P. Zhuang, Phase diagram of a cold polarized Fermi gas in two dimensions, *Phys. Rev. A* **78**, 033613 (2008).
- [47] S. N. Klimin, J. Tempere, and J. T. Devreese, Pseudogap and preformed pairs in the imbalanced Fermi gas in two dimensions, *New J. Phys.* **14**, 103044 (2012).
- [48] M. M. Parish and J. Levinsen, Highly polarized Fermi gases in two dimensions, *Phys. Rev. A* **87**, 033616 (2013).
- [49] D. E. Sheehy, Fulde-Ferrell-Larkin-Ovchinnikov state of two-dimensional imbalanced Fermi gases, *Phys. Rev. A* **92**, 053631 (2015).
- [50] U. Toniolo, B. Mulkerin, X.-J. Liu, and H. Hu, Larkin-Ovchinnikov superfluidity in a two-dimensional imbalanced atomic Fermi gas, *Phys. Rev. A* **95**, 013603 (2017).